Urban Forestry & Urban Greening 59 (2021) 127002

Contents lists available at ScienceDirect

Urban Forestry & Urban Greening

journal homepage: www.elsevier.com/locate/ufug

The effect of stem and root-plate defects on the tree response during static loading—Numerical analysis

Barbora Vojáčková [a,*], Jan Tippner [a], Petr Horáček [a,b], Václav Sebera [a,c], Luděk Praus [a], Robert Mařík [d], Martin Brabec [a]

[a] Department of Wood Science and Technology, Mendel University in Brno, 613 00, Czech Republic
[b] Department of Water Operation and the Creation and Allocation of Biomass, CzechGlobe CAS, 603 00, Czech Republic
[c] InnoRenew CoE, 6310, Izola, Slovenia
[d] Department of Mathematics, Mendel University in Brno, 613 00 Czech Republic

ARTICLE INFO

Handling Editor: Gregory Dahle

Keywords:
Pulling test
Tree stability
Stem strain
Root-plate inclination
Stem deflection
Finite element method
Taylor approximation

ABSTRACT

Despite continual development of the tree pulling test, there is no systematic study on the interaction of stem and root-plate stiffness in relation to tree assessment results. New methods involving numerical modelling and optical techniques provide tools for effective and deeper understanding of the interaction of stem and root-plate stiffness. Within this study, a finite element (FE) model of the tree response to static loading was developed, and the interaction between the stem and root-plate stiffness was analysed on three levels: longitudinal stem strains, root-plate inclinations and stem deflection curve. The model was validated at all three levels by comparison with experiment. Sensitivity analysis of the validated model showed a significant correlation of root-plate stiffness represented by the root volume and soil elastic modulus to the tree response. By analysing the defects in tree response, the importance of proper location for detection of strains and inclinations was demonstrated, especially regarding asymmetrical defects. A numerical estimate of the second derivative of displacement based on the Taylor approximation, was used to analyse the stem deflection curve.

1. Introduction

Trees are fundamental to health of urban environments. As the public starts to become aware that trees are an essential part of our well-being, tree owners and managers are facing liability for tree failures (Mortimer and Kane, 2004). In general, tree risk assessment is a combination of the probability of tree failure, impact potential and the target value (Ellison, 2005). A range of methods for assessment of tree failure probability have been developed (Wessolly and Erb, 2016; Dahle et al., 2017) including pulling tests (Peltola, 2006; Detter and Rust, 2013). The pulling test, which is used to assess resistance to stem breakage or uprooting was developed in the form of the elasto-inclino method (Brudi and van Wassenaer, 2001). This method measures the longitudinal strains in stem and root-plate inclinations and is consequently used to evaluate stem breakage and uprooting resistance (Brudi and van Wassenaer, 2001; Detter et al., 2002; Wessolly and Erb, 2016). The data regarding strains and inclinations is processed separately, which raises the question of the relationship between the stiffness of the stem and root-plate. This relationship can affect the results of the elasto-inclino method and has not been investigated yet. Neild and Wood (1999) provided a study of the iterative procedure for calculating deflection curve, which helps determine stem and root-plate stiffness. Their study highlights the importance of both root anchorage and stem flexibility for a better prediction of stem deflection. The stem deflection curve was measured in an experimental study by Lundström et al. (2007). This study used stem displacement to calculate the predicted contribution of overhanging tree weight to its turning moment. Stem deflection was obtained by image analysis, which enabled tracking of the entire stem (Jonas and Lundström, 2005). Optical techniques based on digital image correlation (DIC) are potential tools, due to information from the vast amount of points (markers) is obtained both in 2D or 3D form (Sutton et al., 2009; Tippner et al., 2019). This allows for the possibility to observe larger tree parts by using marker tracking (Vojáčková et al., 2019) and provides the opportunity to obtain full-field information (Sebera et al., 2014, 2016).

The ability of full-field optical techniques to reveal the stem defect, root-plate damage and their combination has been studied by Tippner et al. (2019). This study proved that optical technique provides

* Corresponding author at: Zemědělská 3, 613 00, Brno, Czech Republic.
E-mail address: barbora.vojackova@mendelu.cz (B. Vojáčková).

https://doi.org/10.1016/j.ufug.2021.127002
Received 2 April 2020; Received in revised form 11 December 2020; Accepted 19 January 2021
Available online 28 January 2021
1618-8667/© 2021 The Author(s). Published by Elsevier GmbH. This is an open access article under the CC BY license (http://creativecommons.org/licenses/by/4.0/).

comparable results to extensometers and suggest that there is an interaction between defects (to each other) and to different position of measurement. The separate impact of stem defect and root-plate damage was studied by Smiley et al. (2014, 2012) and Smiley (2008) who found a nearly linear decrease in the stiffness with increasing damage size. In these studies similar to the research conducted by Ciftci et al. (2014), tree response was measured locally at the position of the defect or above.

As a supplement to experimental techniques, the finite element method (FEM) is a promising tool for mechanical analysis of defects interaction and tree behaviour. The FEM has already been used to observe root breakage (Yang et al., 2014) and overturning processes (Rahardjo et al., 2014) with connection to soil conditions (Dupuy et al., 2005; Jonsson et al., 2006). FE analysis varies from models with simplified geometry (Fourcaud et al., 2008; Khalilnejad et al., 2012) to complex models of accurate root geometry that aim to find the significant parameters of tree anchorage. Gaffrey and Kniemeyer (2002) developed the 3D FE model to estimate stress and strain distribution on the stem surface. Regardless of its simplification level, the FEM allows input parameters to be defined and provides data set information on a level similar to the one obtained by optical techniques. The combination of the FEM and DIC can help to understand the interrelation within the tree in a broader context because of the opportunity to observe the behaviour of a number of positions at one moment and compare the theoretical results with the experimental results. The main goal of this study is to analyse the influence of defects to the stem response while considering the interaction between the stiffness of the stem and root-plate. The concept of this study consists of: a) development and validation of a reasonably complex FE model to simulate tree response to static loading, similar to the assessment provided by the pulling test, b) sensitivity analysis of a wide range of parameters influencing tree response to loading, c) analysis of defects and their influence on strains, inclinations and the deflection curve. The results of the FE model will then be compared and analysed on three levels including strains, inclinations and deflection curve. This data can be obtained by the elasto-inclino method or by optical techniques.

2. Methods

2.1. FE model and validation

The tree species *Aesculus hippocastanum* L. (common name horse chestnut) was measured to obtain the data for validation of the FE model regarding tree response. The measured tree had two stems growing closely side by side. One of the stems was colonised by tinder fungus (*Fomes fomentarius* L.) and the tree had low vitality. The stem with no symptoms of infection or damage was chosen for the experiment. For safety reasons, the stem with fungus and the healthy stem's crown were removed before testing. The tree's diameter at breast height was 60 cm. The diameter of the root-plate, representing the soil–root complex, was 1.2 m, and the depth was 0.65 m. The dimensions of the root system were gathered by using measuring tape directly after the destructive part of the test, which involved overturning the tree. The shape of the root system was typical for urban trees planted in a nursery without tap root. The tree was located in an open central area of an urban park. The chosen tree was growing without the influence of neighbouring trees and was surrounded by lawn without any sign of compaction. The soil conditions were investigated from the soil pit, and a sandy-clay texture merging to clay was found (FAO, 2006).

The standard pulling test (Brudi and van Wassenaer, 2001) using elasto-inclino measurement was conducted with the addition of optical measurement (Fig. 1). The load was applied by a manually operated winch and recorded by a load cell (Isetron M-0060-1/50 -GE). During the measurement, the stem base inclination was tracked so it could not go beyond an angle of 0.25° to ensure the elastic range of deformation. Stem inclination is composed by the rotation of root-plate and stem inclination. Closer to the ground the root-plate inclination starts to prevail. The inclinometers (Sitall STS 110, precision 0.001°), were placed at ground level (θ_1 – at the neutral axis, θ_2 – at the leeward side) and it was assumed that the measurement represented the root-plate inclination for the following study. The longitudinal strains (ε_1 – on the compression side, ε_2 – on the tension side) were measured by extensometers (Mesing T101 F, precision 0.01 μm). The data-logger DEWE 43 (controlled by Dewesoft 7.0) was used for data collection with an acquisition rate of 10 Hz. During the test, images of the stem and root-plate were captured by a Canon EOS 700D camera continuously taking photos at a rate of 0.2 fps. The camera was placed perpendicular to the pulling direction. The 16 stem markers were painted in a row along the neutral axis and placed 30 cm apart from each other. The square metal markers (10 × 10 cm, with pattern) were placed at the soil surface perpendicular to the camera. Based on the images, the marker displacement was analysed using DIC (MercuryRT 2.7, precision 0.18 mm). The stem (u_{stem}) and root-plate ($u_{root\text{-}plate}$) displacements were used for the validation of deflection curves, representing stem and root-plate deflections.

The parametric linear static structural model of the tree mechanical response was built using FE software ANSYS (Mechanical APDL v. 18.0). The model is three-dimensional with simplified stem and root-plate geometry (Fig. 2). The stem and root-plate geometry were created using 192 segments in total, which consist of (6 + 6) × 12 stem segments plus 4 × 12 root-plate segments. To each segment was given a unique material number, which allowed for the material model to be set for each part to independently simulate defect or material variability. The stem geometry was built to the height of anchorage (h_t 9.2 m) by six inner and six outer frustums (inner frustums are 0.1 m thinner in

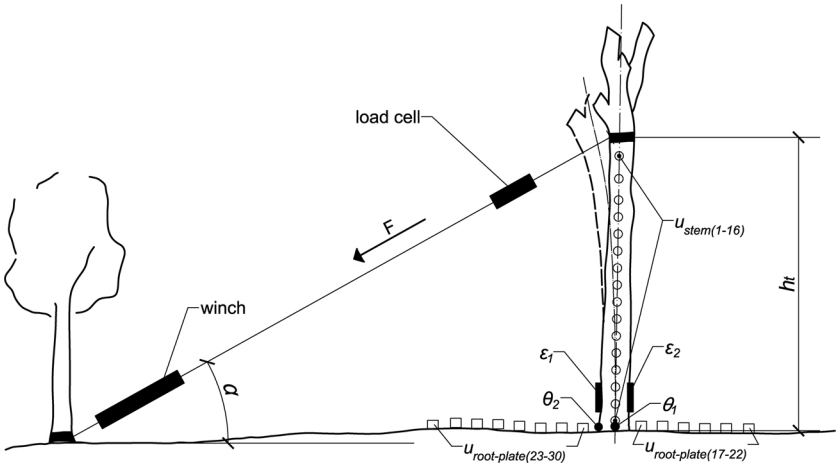

Fig. 1. Measurement scheme: θ_1, θ_2 are inclinations measured by inclinometers placed at a height of approx. 0.05 m. ε_1, ε_2 are longitudinal strains measured by extensometers placed at a height of approx. 0.6 m. $u_{stem(1\text{–}16)}$ are the stem displacements at the position of markers placed from the tree base to the anchorage point and $u_{root\text{-}plate(17\text{–}30)}$ are the root-plate displacements at the position of markers placed approx. 3.5 m from the tree base. α is the angle of the line anchorage. h_t is the height of cable attachment (9.2 m above the ground level, which is approximately 50 % of the overall tree height). F is applied force.

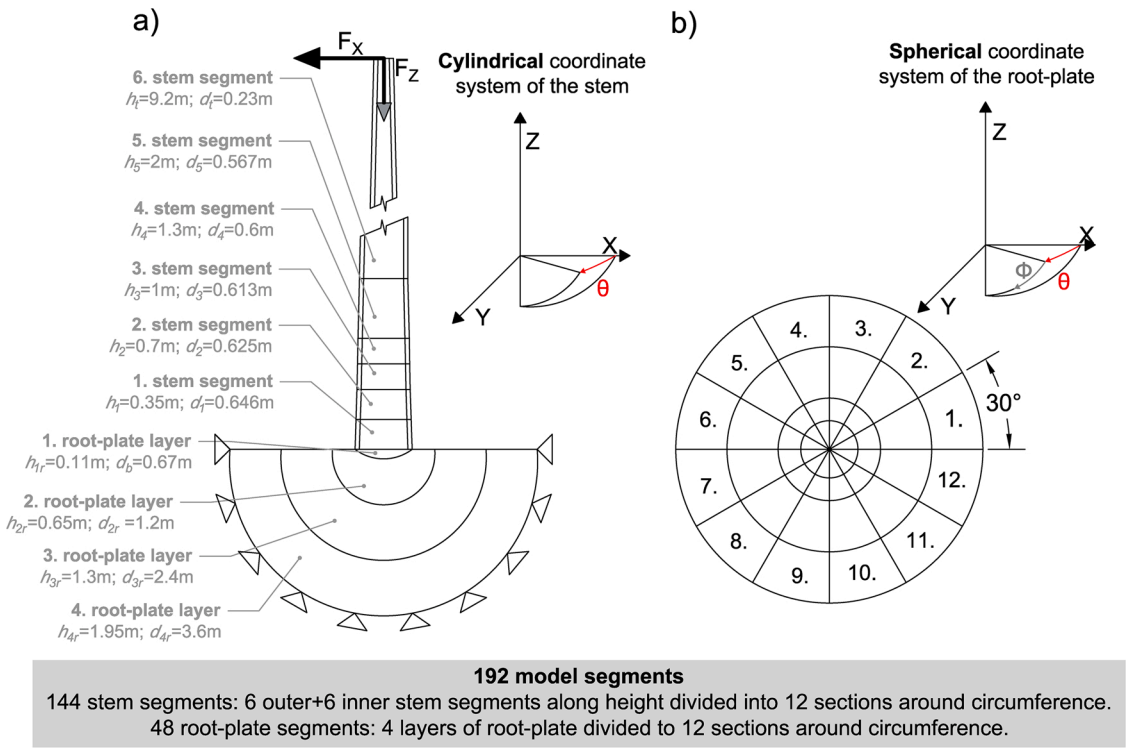

Fig. 2. Scheme of the model: a) front section view with boundary conditions, *h(i)* is the height of the segment at the top and *d(i)* is the diameter of the stem without bark or root-plate diameter in the top part of the segment. F_x, F_z are applied forces; b) the circular plan view shows the stem and root-plate divided into 12 sections.

diameter). The diameter of each frustum was calculated according to previously measured ones (stem base d_b, breast height d_{bh}, positions of extensometers d_e). The taper function was calculated between two consecutive measured diameters and then used to calculate the diameters in defined heights (Fig. 2).

The root-plate was made up by four layers comprised of spherical segments and then divided into 12 sections around the circumference to create spherical wedges in each layer. The spherical shape represented the typical root system of a tree in an urban environment where the species-specific shape is usually suppressed by nursery treatments and variable conditions. The diameter of the first layer of root-plate was equal to the d_b and the depth was 1/3 of the stem base radius. The dimensions of the second layer were 1.2 m in diameter and 0.65 m deep according measurement. The third layer was two times bigger than the second layer, and the fourth layer was three times bigger than the first layer.

The orthotropic material model of green wood for the stem was based on the modulus of elasticity (*MOE*) assigned from the pulling test and data from Kretschmann (2010). The *MOE* was derived from a standard stress–strain diagram composed of measured strains (ε_1, ε_2) and calculated stress. The stress was calculated from the modulus of cross sections at the position of the extensometers (h_1, h_2) and bending moments (M_1, M_2) by using the following equation:

$$M_i = F\cos\alpha(h_t - h_i) \quad (1)$$

The calculated *MOE* (5800 MPa) represents the longitudinal elastic modulus (E_L). The radial (E_R), tangential (E_T) and shear moduli (G_{LR}, G_{LT}, G_{RT}) were calculated from the E_L using ratios of the elastic modulus for *Tilia americana* L. (common name basswood), which were published by Kretschmann (2010) (Table 5-1). Poisson's ratios (μ_{RL}, μ_{TL}, μ_{TR}) were also adopted from Kretschmann (2010), (Table 5-2). Data for the green wood density of *Aesculus hippocastanum* L was set to 880 kg/m^3 according to Kretschmann (2010) (Table 4-6a). This approach assumes comparable properties of *Tilia americana* L. and *Aesculus hippocastanum* L. corresponding to similar densities and *MOE* presented by Kretschmann (2010). The effect of moisture content on elastic ratios was neglected.

The isotropic material model of the root-plate system was defined as a composite of root and soil using the rule of mixtures, therefore enabling a different portion of soil and roots to be present in each layer. The first layer contained 70 % roots, the second layer contained 20 %, the third layer contained 5% and fourth and final layer was pure soil. The elastic modulus of soil (E_{soil}) was chosen to be 20 MPa and Poisson's ratio was set to 0.3 (Bowles, 1997; Dupuy et al., 2007). The soil density was set to 2500 kg/m^3 based on measured properties. The elastic moduli for the roots were considered to be the same as the stem wood in the first layer, in the second layer they were reduced to 50 % and in the third layer to 25 %. The model was meshed with tetrahedron elements because of its complex geometry (Fig. 3).

The boundary conditions for root-plate fixing were defined as having zero displacements in all three directions on the outer area the fourth layer (Fig. 2). The loading of the model was divided into 11 steps. The first step consisted of the self-weight effect represented by vertical (Z direction) acceleration for all elements to simulate gravity. The following ten steps simulated linear increments of pulling force up to 8665 N, which was the experiment's maximal value. The force was divided into the F_X and F_Z components according to α. For the FE model validation, the effect of the crown was not included according experiment. For the following analyses, the effect of the crown was applied as vertical force on the surface of the top stem cross-section.

Validation of the model was based on a comparison of the stem longitudinal strains (ε_1, ε_2), root-plate inclinations (θ_1, θ_2) and deflections (u_{stem}, $u_{root\text{-}plate}$). u_{stem} and $u_{root\text{-}plate}$ were compared at the maximum load level by relative errors (*RE's*) of each observed point. Comparison of the ε_1, ε_2 and θ_1, θ_2 was based on the interpretation of M_i vs. ε_i and M_i vs. θ_i data by linear functions (linear regression model), where the slopes of these functions represent stem and root-plate stiffness (Jonsson, 2006; Neild and Wood, 1995). M_i was calculated according Eq. (1) for each corresponding position of ε_i and θ_i. The validity

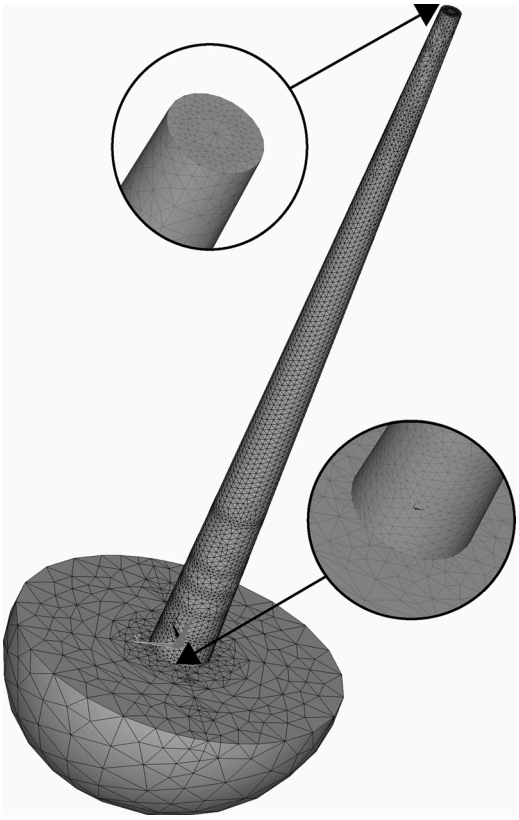

Fig. 3. The FE model with quadratic tetrahedron elements (SOLID187) and detailed mesh connections (consists of 77469 nodes).

of experimental data interpretations using linear functions based on a FE model was evaluated by a coefficient of determination (R^2). Thus R^2 describes how the linear regression model of stem and root-plate stiffness corresponds to the measurement.

2.2. Sensitivity analysis (SA)

The sensitivity analysis (*SA*) aims to provide a general overview of the tree response to varying parameters. The results were compared with experimental findings from the literature to validate the functionality of the model (Table 1). Parametric definition of the model allowed a broad series of tests to be performed in order to investigate the influence of changes in geometry and material on $\theta_{1,2}$ and $\varepsilon_{1,2}$ used in the practice of tree pulling assessment. It also described the effect of changing tree parameters on $u_{root\text{-}plate}$ and u_{stem} at different heights (<1 *m, 1–1.8,* >4.5 *m*).

The SA was performed by ANSYS Probabilistic Design System and was based on the randomised generation of the input parameters by the Monte Carlo method. The ten input parameters representing shape and material properties of the stem and the root-plate were tested (Table 1). Selection of the input parameters and their range were both configured according to the preliminary sensitivity analyses, by taking the data available in the literature and parameters available during common field survey into consideration. The SA counted 300 computational cycles. The significance of the input to the output parameters was described by Spearman correlation coefficients (ρ; $\alpha < 0.05$).

2.3. Impact of defects on strains, inclination and deflection curve

An advantage of the segments in the FE model is ability to investigate the influence of internal defects on tree response during loading. Two common kinds of defect were considered: decay in the stem and root damage (Fig. 4). Stem decay was represented by the reduction of elastic

Table 1
Description and range of input parameters of SA including the explanation of selected values.

Description	Range of values in SA	Explanation to chosen range of parameters	Parameter considered as a significant by
stem tapering (t)	0.01−0.02	allowed by model dimensions	Spatz and Bruechert (2000)
stem base diameter (d_b)	±5%	allowed deviation in diameter measurement according to Kolařík et al. (2018)	Lundström et al. (2007); Smiley (2008)
the depth of static significant root-plate (h_{r2})	$1/2d_b$-d_b	the correlated depth of root-plate, according to Mattheck and Breloer (2003)	Moore (2000); Ghani et al. (2009)
the diameter of static significant root-plate (d_{r2})	1.3−2.8 m	minimum possible dimension to the maximum value computed according to Mattheck and Breloer (2003)	Moore (2000); Ghani et al. (2009)
*amount of root volume in the first layer (r_1)	50−90%	estimation of root volume in different distances from stem	Crook and Ennos (1996); Coutts (1986)
*amount of root volume in the second layer (r_2)	10−70%		
longitudinal elastic modulus at stem base (E_{L1})	5200−9400 MPa	the range of literature values Kretschmann (2010); Wessolly (1996); Lavers (1983)	Niklas (1992); Wessolly (1995); Gross et al. (2011)
longitudinal elastic modulus to 1 m (E_{L2})	5200−9400 MPa		
longitudinal elastic modulus over 1 m (E_{L3})	5200−9400 MPa		
elastic modulus of soil (E_{soil})	20–500 MPa	the range of literature values Dupuy et al. (2007); Fourcaud et al. (2008); Bowles (1997)	Coutts (1986); Moore (2000); Dupuy et al. (2007); Kamimura et al. (2011)

* Considering the root-plate defined as a composite of roots and soil, the root volume was varied to represent the influence of the root properties in the root-soil complex.

moduli to 10 % of its original value in the inner stem segments. To simulate root system damage, the elastic modulus of the roots was reduced in the second and third layer to 10 % of the original value.

Two approaches were used to evaluate the influence of defects: a comparison of slopes between M_i vs. ε_i and θ_i to observe the influence of the elasto-inclino method, and a comparison of the stem deflection curves, which represent the overall response to the changes in stem and root-plate stiffness. The effect of the defects was investigated by taking the first and second derivatives of the stem deflection equation, which is an approach commonly used for cantilevered beams. The first derivative of stem deflection as a function of height equals the stem inclination while the second derivative describes the curvature. The progress of first (Eq. (2)) and second derivative (Eq. (1)) of displacement to stem height was used. The second derivative was evaluated from three consecutive nodes (see the formula (2) below) and this quantity was chosen in order to compare the stem deflection to the theoretical deflection of a uniform homogeneous beam.

An approximation based on the Taylor approximation was used to obtain the second derivative of the function *u(h)* (Riley et al., 2006). The classical approach was adjusted for the purpose of managing non-uniform steps in the stem height (h). The following second-order formula for the second derivative of the function given by a discrete

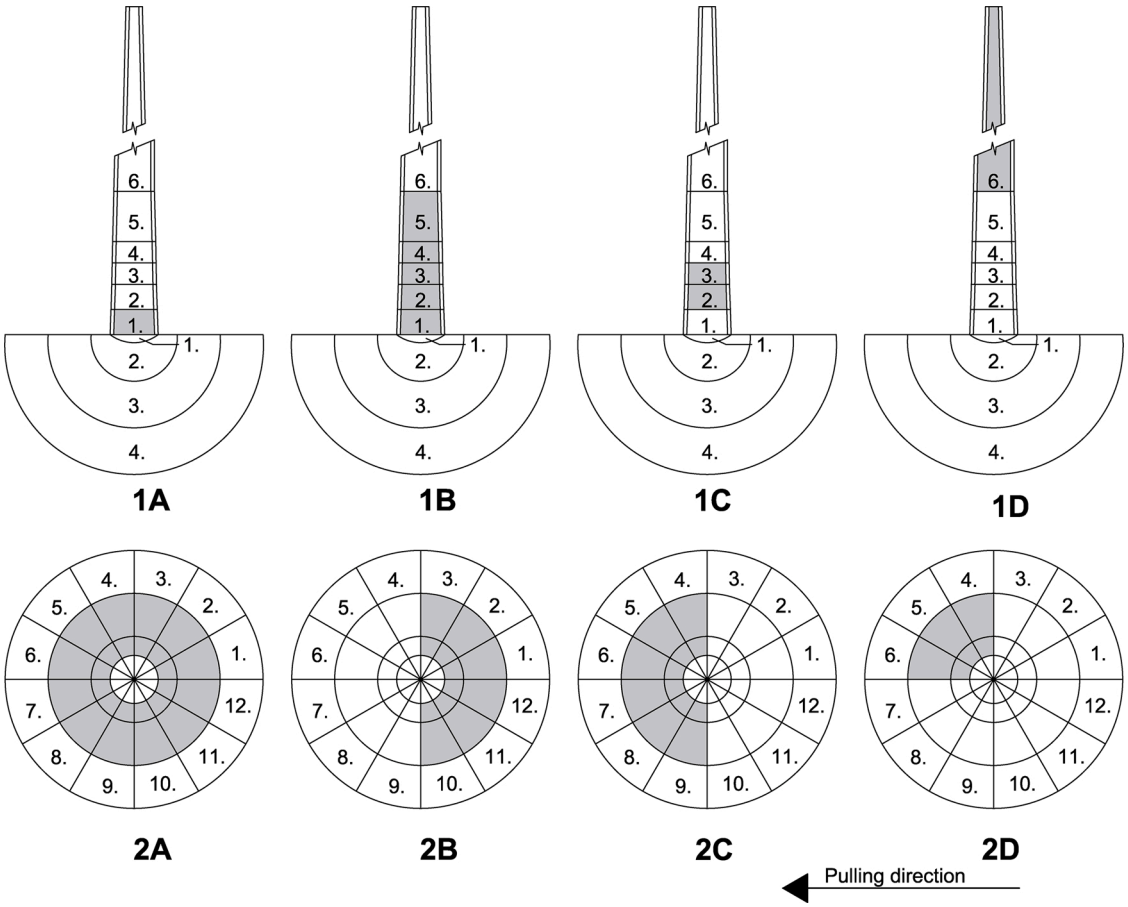

Fig. 4. Schema of the defects. The grey area represents stem defects and root-plate damage. 1A) the base of the stem (up to 0.35 m), 1B) the lower part of the stem (up to 2 m), 1C) the middle part of the stem (from 0.35 to 1 m), 1D) the upper part of the stem (from 2 to 9.2 m). 2A) the whole root system, 2B) the windward side of the root system, 2C) the leeward side of the root system, 2D) 1/4 of the root system on the leeward side.

set of data points $u(h_{i-1}) = u_i$ was obtained.

$$u''(h_i) \approx 2\frac{u_{i+1}(h_i - h_{i-1}) + u_{i-1}(h_{i+1} - h_i) - u_i(h_{i+1} - h_{i-1})}{(h_{i+1} - h_i)(h_i - h_{i-1})(h_{i+1} - h_{i-1})} \quad (2)$$

The second derivative $u''(h_i)$ was multiplied by the fourth power of the diameter (d_i) in all analysed positions to include the cross-section influence of the response. The order power was chosen as a result of dimensional analysis and the Buckingham-Pi theorem (Simon et al., 2017), which relates the quadratic momentum and fourth power of dimensions.

The numerical estimate of the first derivative of the deflection was used as a supplementary tool in plotted diagrams. First derivative was evaluated as a forward difference by the following formula:

$$u'(h_i) = \frac{(u_{i+1} - u_i)}{(h_{i+1} - h_i)} \quad (3)$$

3. Results

3.1. FE model and validation

Simulated ε_1, ε_1, θ_1, θ_2 and u_{stem}, $u_{root\text{-}plate}$ were compared with data from the mechanical sensors and marker tracking. Fig. 5 shows the difference between experimental devices and the FE model results. The nearly symmetrical response of the model did not fit the measurements, which yielded different results according to the device positions. The asymmetrical response of measurement caused a lower R^2 for modelled θ_2 (0.74) and ε_1 (0.45), while the R^2 for θ_1 was 0.92 and ε_2 was 0.9.

The relative errors (*RE*) between the model and the measured u_{stem} ranged from -14 to -33 % with an average of 22 % and variation of 22 %. The RE between the model and the measured $u_{root\text{-}plate}$ ranged from 35 to -90 % (Fig. 6). The negative values of *RE* show that the displacement of the FE model was lower than the measurement, with the exception of displacement on the windward side of the root-plate. The points closest to the tree base ($u_{root\text{-}plate17}$ and $u_{root\text{-}plate23}$, Fig. 1) were excluded from the validation because they were partially connected to the stem and did not provide representative results of $u_{root\text{-}plate}$.

3.2. SA outputs

Significant correlations from *SA* are gathered together in Table 2. The root volume in the first (r_1) and second (r_2) layer was in negative correlation to θ_1, θ_2 and u_{stem}. The influence of r_2 on θ_1 and θ_2 (ρ = 0.76–0.77) and u_{stem} (ρ = 0.4–0.7) is one of the most significant in the frame of the model. Similarly, elastic modulus of soil (E_{soil}) is the parameter that significantly influences the majority of the output parameters ($\rho > 0.5$), except for the displacement in the upper part of stem ($u_{stem>4.5m}$). The depth and diameter of the root-plate (hr_2, dr_2) are less significant parameters in comparison to root and soil properties (represented by the r_1, r_2 in the modelled composite). Significant correlation was found between the $u_{root\text{-}plate}$ and depth of root-plate system (h_{r2}); the correlation is higher on the windward side (ρ = 0.38–0.75) and decreases with distance from the stem. On the leeward side, the correlation is generally lower (ρ = 0.13–0.48) and increases with distance from the stem.

Considering the parameters of stem, the diameter (d_b) has a higher influence on u_{stem} and θ_1, θ_2 than the elastic moduli (E_L). The influence of stem diameter on displacement increases with height (from ρ = 0.15 at

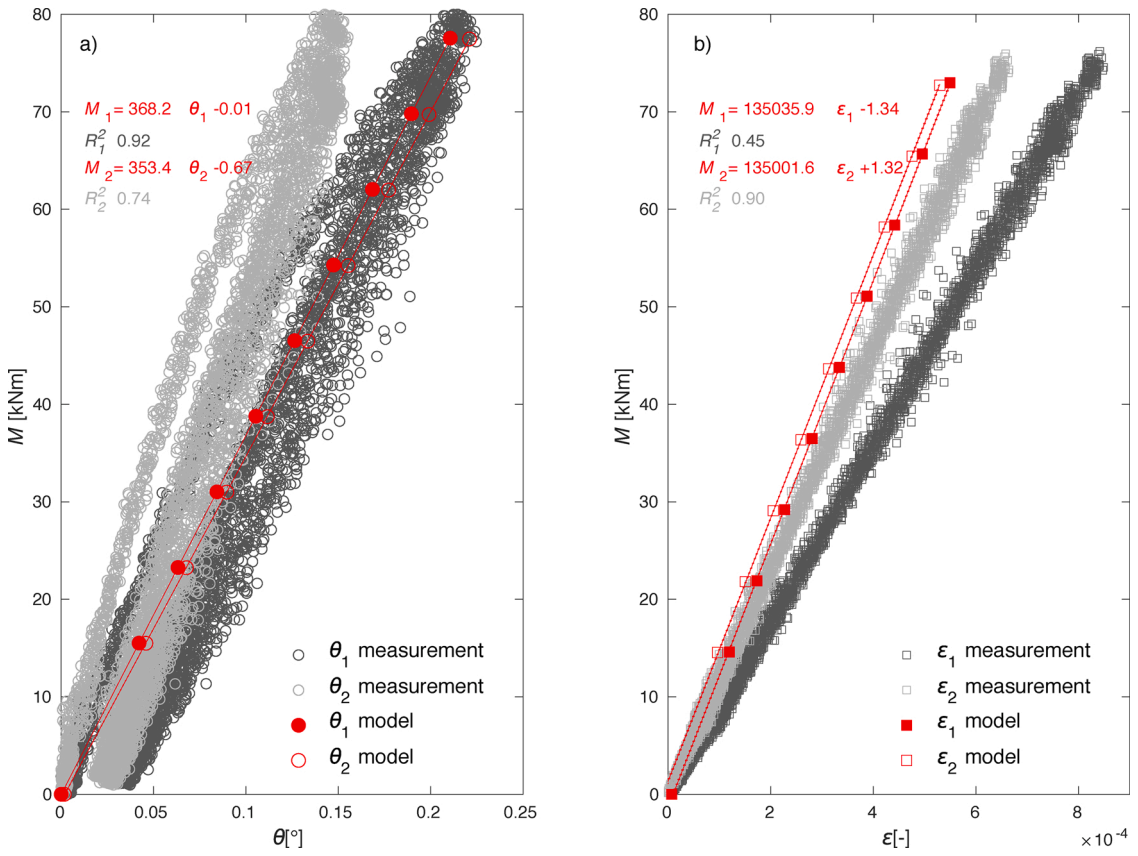

Fig. 5. Comparison of the elasto-inclino measurement and model results: a) root-plate inclination θ_1 – at the neutral axis, θ_2 – at the leeward side; b) stem strain ε_1 – at the compression side, ε_2 – at the tension side; $M_{(1,2)}$ - bending moment at the position of devices; $R^2_{(1,2)}$ coefficient of determination for corresponding device.

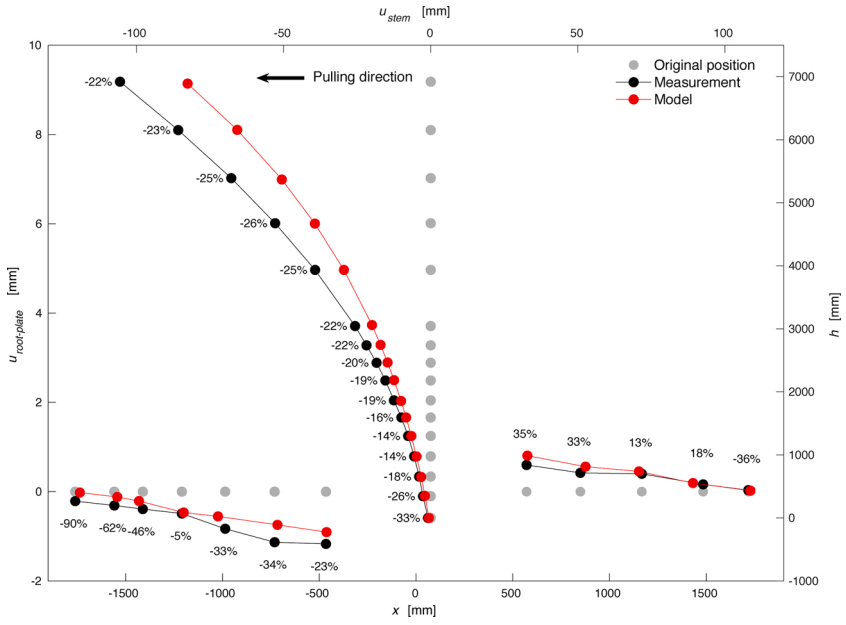

Fig. 6. Scaled diagram of stem and root-plate deflection with relative errors between the model and the measured displacements at corresponding positions of the tree: u_{stem} is the stem displacement, $u_{root\text{-}plate}$ is the root-plate displacement, h is the stem height and x is the position on the ground.

the base to $\rho = 0.59$ at height above 4.5 m), which is supported by the significance of tapering (t), which occurs exclusively in the higher part of the stem (Table 2). The highest correlations ($\rho = 0.87$–0.89) were found for the elastic modulus (E_{L2}), changes in the range of values for sound wood, and longitudinal strains ($\varepsilon_{1,2}$) near the position of these changes. In general, the horizontal displacements used for the deflection curve definition were less correlated with the changes of E_L ($\rho = 0.11$–0.41).

Table 2
Significant Spearman's correlation coefficients. The range of coefficients is grouped according to the position at the tree (root-plate inclination $\theta_{1,2}$, root-plate displacement $u_{root\text{-}plate}$, stem strains $\varepsilon_{1,2}$ at the position of extensometers, stem displacement below 1 m $u_{stem<1m}$, from 1 to 1.8 m $u_{stem1\text{-}1.8m}$ and above 4.5 m $u_{stem>4.5m}$). For a description of input parameters see Table 1. The values higher than 0.5 are bolded.

Parameter	$\theta_{1,2}$	$u_{root\text{-}plate}$	$\varepsilon_{1,2}$	$u_{stem<1m}$	$u_{stem1\text{-}1.8m}$	$u_{stem>4.5m}$
t						0.18–0.35
d_b	-(0.25–0.26)	-(0.13–0.15)	-(0.45–0.49)	-(0.15–0.35)	-(0.41–0.43)	**-(0.58–0.59)**
h_{r2}	-(0.17–0.16)	**-(0.13–0.76)***		-(0.12–0.13)		
d_{r2}	-(0.21–0.22)	-(0.21–0.41)		-(0.2–0.3)	-(0.17–0.18)	
r_1	-(0.15–0.16)			-(0.13–0.14)	−0.12	
r_2	**-(0.76–0.77)**		-(0.14–0.18)	**-(0.46–0.72)**	**−0.7**	**-(0.4–0.52)**
E_{L1}	-(0.13–0.16)			-(0.17–0.2)	−0.2	-(0.15–0.11)
E_{L2}	-(0.11–0.12)		**-(0.87–0.89)**	-(0.11–0.2)	-(0.25–0.26)	-(0.15–0.21)
E_{L3}						-(0.32–0.41)
E_{soil}	**-(0.52–0.53)**	**-(0.69–0.92)**		**-(0.55–0.83)**	**-(0.51–0.52)**	-(0.32–0.41)

* The correlation on the windward side is higher than on the leeward side.

3.3. Impact of defects on strains, inclination and deflection curve

The validated FE model by comparison with measurement and *SA* was used for the analysis of defects. The effects of root-plate damage to θ_1 and θ_2 are presented in Fig. 7. The highest increase of inclinations was naturally caused by symmetrical damage of the whole root system (2A). There was no difference between θ_1 and θ_2. The θ_2 was higher for damage on the leeward side of the tree (2C) than for damage on the windward side (2B). While θ_1 increased about the same value for damage on the windward (2B) and leeward (2C) sides of the tree.

The slight increase in θ_1 was caused by a defect in the lower part of the stem (1A) and decrease by a defect in the middle part of stem (1B). The opposite reaction occurred for θ_2.

The $\boldsymbol{\varepsilon_1}$ and $\boldsymbol{\varepsilon_2}$ increased in the case of stem defects (1A) located under the place of strain evaluation (Fig. 8). The stem defects found above the position of strain evaluation (1D) caused only a slight increase of $\boldsymbol{\varepsilon_1}$ and $\boldsymbol{\varepsilon_2}$.

The asymmetric root-plate damage significantly influenced strains (Fig. 8). Damage on the windward side (2B) caused an increase of ε_1 and decrease of ε_2, while damage on the leeward side (2C) induced the opposite response. The impact of ¼ root-plate damage (2D) was similar; ε_2 increased and ε_1 decreased.

The study was complemented by analysis of the influence of the defect position on the stem deflection. Fig. 9 shows the change of the deflection curve for various defect scenarios. The inclination along the whole stem of the damaged root system was higher in comparison to a tree without damage. This observation was supported by the results of the root-plate surface displacement. Contrary to the response of the stem defect, the root-plate damage caused higher inclinations in the bottom part of the deflection curve. The maximal displacement (u_{max}) increased

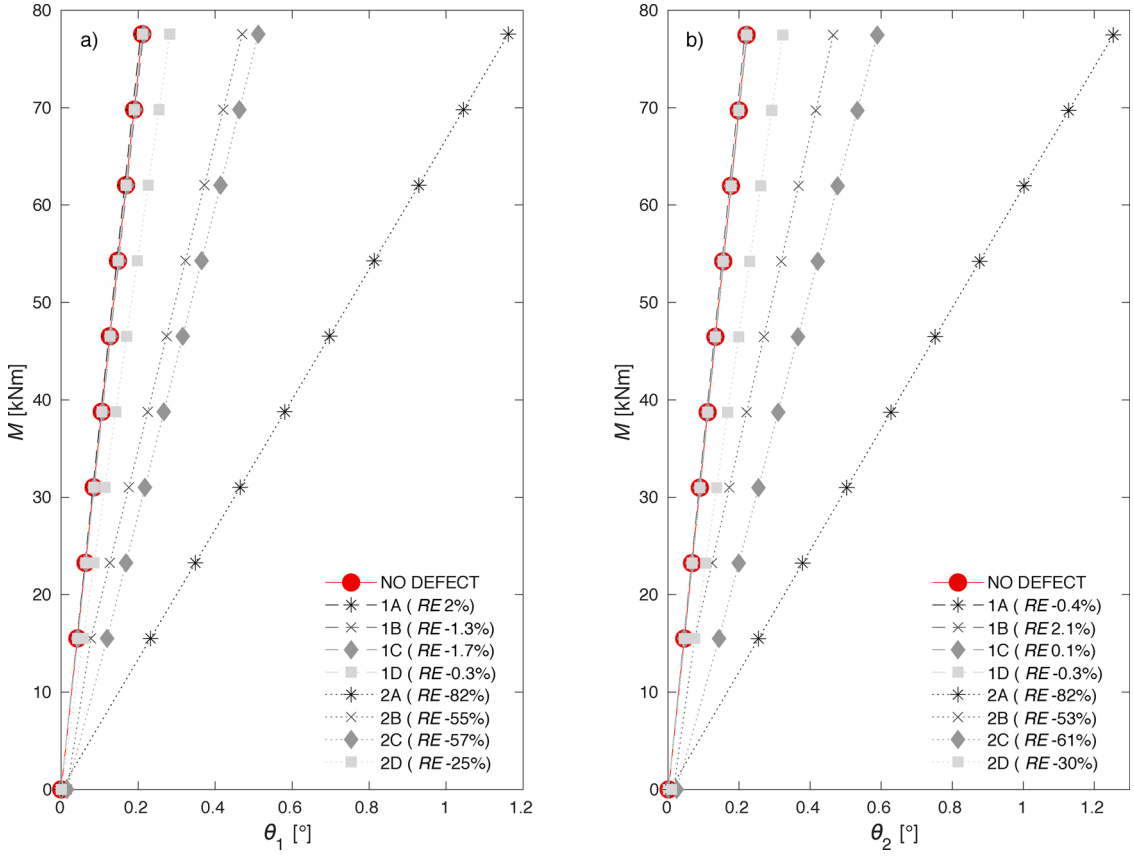

Fig. 7. FE analysis – influence of the stem defects (1A-D, Fig. 4) and root-plate damage (2A-D, Fig. 4) to the root-plate inclinations: a) inclination at the neutral axis (θ_1); b) inclination at the leeward side (θ_2). *RE* represents inclination relative error to the model without defects.

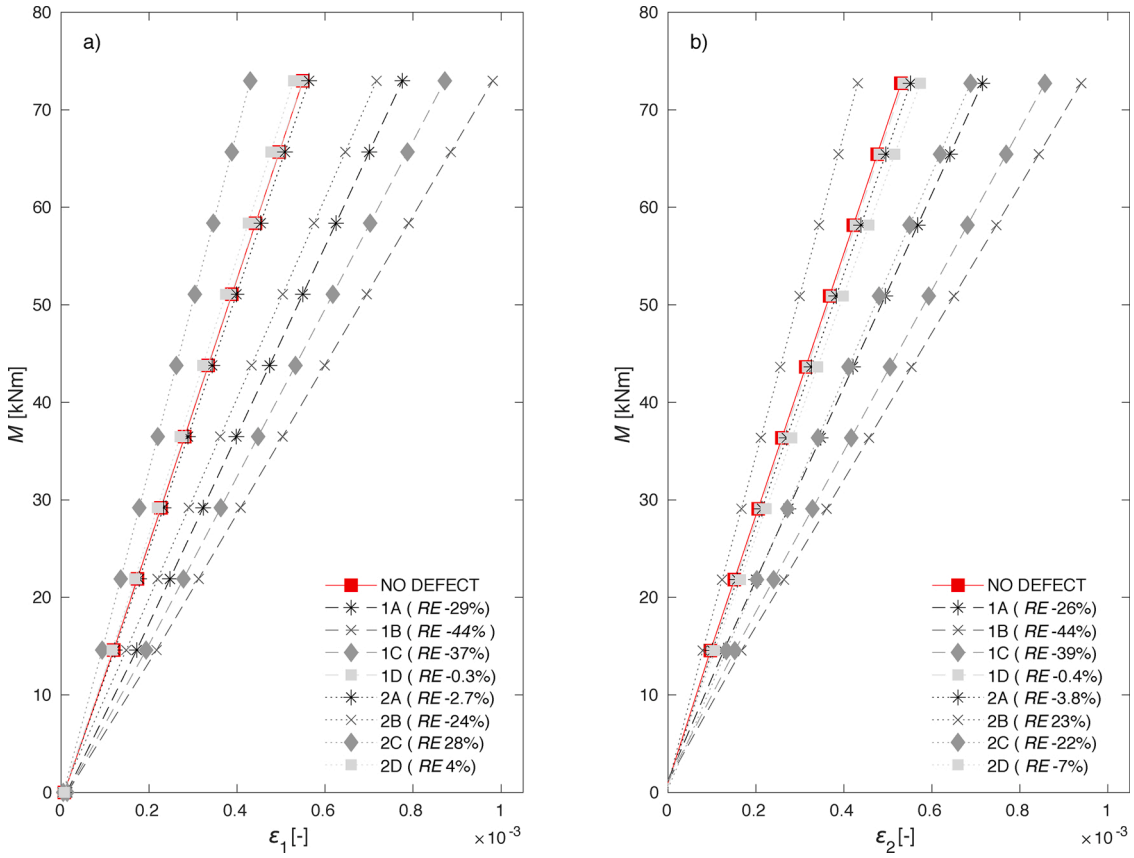

Fig. 8. FE analysis – influence of stem defects (1A-D, Fig. 4) and root-plate damage (2-D, Fig. 4) to the strains: a) compression side (ε_{1}); b) tension side (ε_{2}). *RE* represents strain relative error to the model without defects.

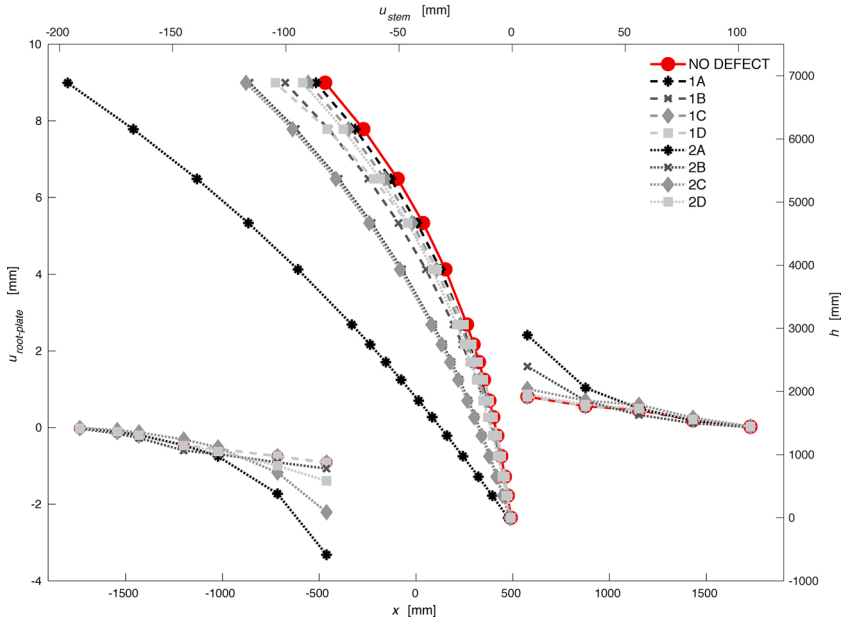

Fig. 9. Deflection curves for various scenarios in defect analysis (1A-D, 2A-D, Fig. 4) at maximum load level: u_{stem} is the stem displacement, $u_{root\text{-}plate}$ is the root-plate displacement, h is the stem height and x is the position on the ground.

about 138 % for damage of the whole root-plate (2A). The displacement also increased 40 % for the windward side (2B), 42 % for the leeward side (2C) root-plate damage and 12 % for the ¼ root-plate damage (2D). The simulated root damage (2A, 2B, 2C) causes greater stem and root-plate displacements then stem defects. Higher $u_{root\text{-}plate}$ occurred at the damaged side (2B, 2C), while the region closest to the stem showed the highest response. As for the stem defects, the largest increase of u_{max} (27 %) was caused by the defect in the upper part of the stem (1D), which is represented by where the deflection curve became straighter at the bottom. For a defect in the lower part (1B), the deflection curve already

inclined in the stem base although the increase in u_{max} was 21 %, which is similar to 1D. The deflection curves of defects in the middle of the stem (1C) and in the base of the stem (1A) overlapped with an increase of u_{max} at 9% and 5%, respectively.

The first and second derivatives of displacements were calculated (Figs. 10 and 11) to detect the differences in stem response for various defects. The first derivative provides an accessible evaluation of defect's presence. Regarding the stem, it is easy to see the change of curve inclination (Fig. 10). The root-plate damage is presented by curve offset (Fig. 11). This evaluation is supported by the second derivative, which detects the defect position through a clear change of the curve course. The theoretical deflection of a beam with constant E_L and uniform cross-section is directly proportional to cube of the length between the fixed end and the point of deflection. Due to the continuous dependence on parameters, similar behaviour is expected for cylindrical tapered beams like the stem in the presented model. In this sense, the large second derivative highlights the points of any irregularity caused by the presence of a defect.

The correspondence between the stem defect and the second derivative is visible in Fig. 10. The highest gradient can be seen in the second derivative at the interface between the defect and sound wood (see A and B in Fig. 10, 1A, 1B, 1C). The defect in the upper part of stem (1D) caused a steep change just below the interface. The low gradient in the regions far from the interface of the defect represents a low deviation of the deflection curve from the cubic function (see 1A, 1B, 1C in Fig. 10). A comparison of a stem with no defect shows the higher inclination of the first derivative above the defect (1D in Fig. 10).

The overall increase of stem inclination caused by root-plate damage can be observed in the first derivative offset in Fig. 11, while the shape of the curve is similar to a tree without damage. This is confirmed by the low deviation of deflection from the cubic curve represented by the second derivative (see points between B and C in Fig. 11). The damage is shown by a significant peak in the second derivative curve (see B points in Fig. 11 2A-2C). In the graph labelled 2D, 1/4 of the root-plate was damaged, similar trend as the undamaged root-plate were shown.

4. Discussion

4.1. FE model and its validation

The θ_1 and ε_2 were chosen as reference parameters for validation of the FE model. The experimentally evaluated values were influenced by the position of the measurement devices (Fig. 5), while the FE model (symmetrical in geometry and material) provided similar values for θ_1, θ_2 and ε_1, ε_2. The difference measured in θ_1 and θ_2 (Fig. 5) was most likely caused by the irregular shape of the stem base. Similarly, the difference in measured strains between $\boldsymbol{\varepsilon_1}$ and $\boldsymbol{\varepsilon_2}$ corresponds to its unconventional shape due to the two-trunk stem and different properties of wood in tension and compression. The small difference between θ_1 and θ_2 in the FE model corresponds with Szoradova et al. (2013), who describes no influence of the position of inclinometers for tree evaluation. These results were observed on trees without signs of defects and without root starts. Also recommendations of Brudi and van Wassenaer (2001) for elasto-inclino method do not make difference for placing of extensometers on tension or compression side.

The displacements along the stem and root-plate show that the FE model is generally stiffer, with the exception of the windward side of the root-plate. Dupuy et al. (2007) described similar behaviour in their work

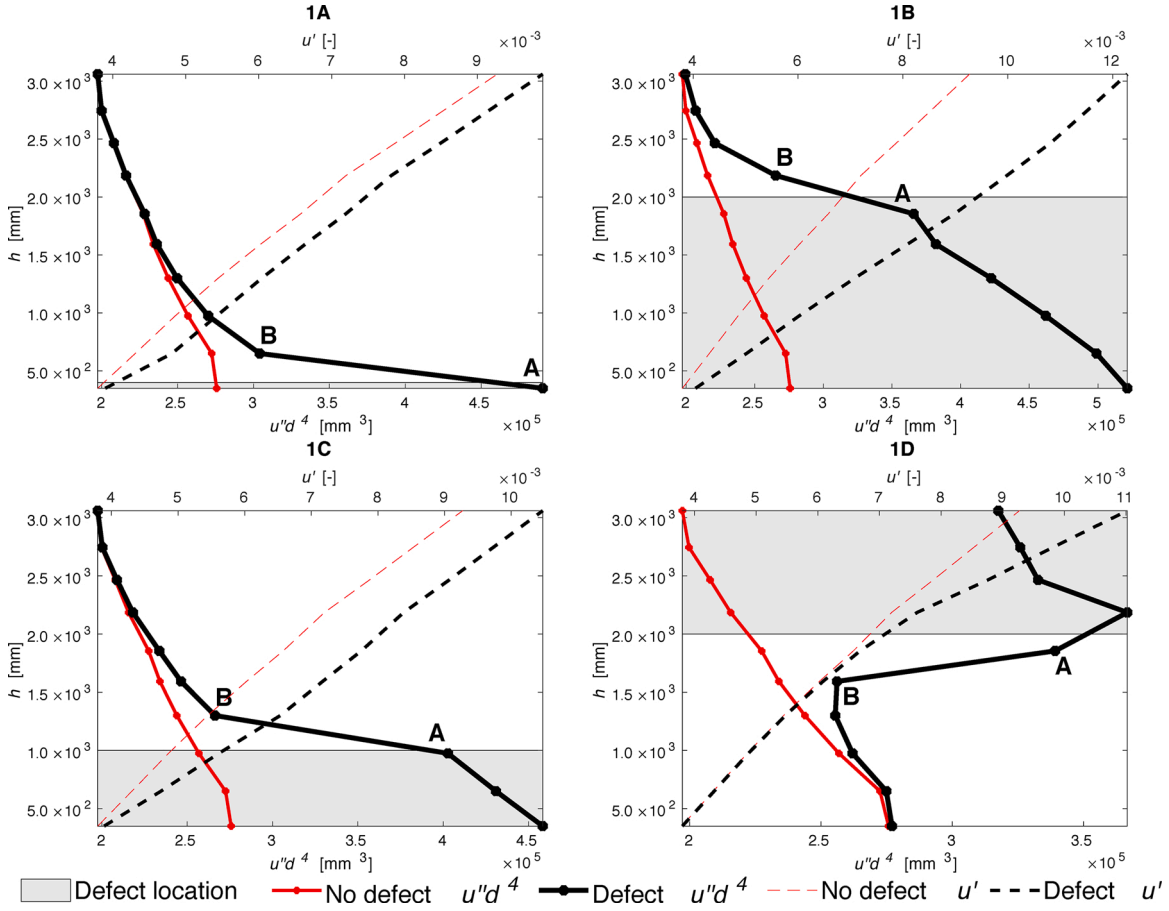

Fig. 10. First and second derivative of u_{stem} for stem defects (1A–D, Fig. 4): $u''d^4$ is the second derivative (Eq. (2)) multiplied by the fourth power of diameter (d_i). u′ is the first derivative (Eq. (3)), h is the stem height. The grey area represents the vertical position of the defect in the stem. A and B are points related to the steep change close to the stem defect.

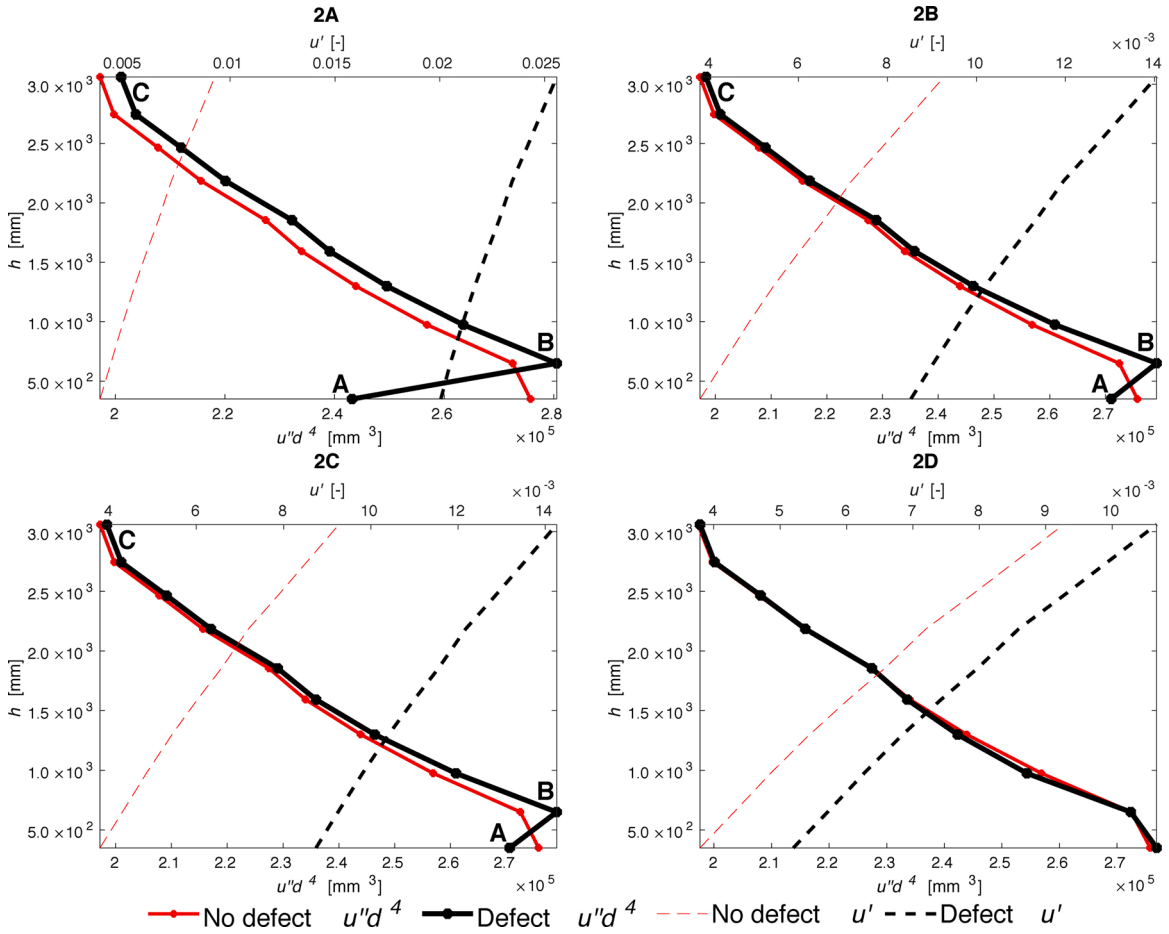

Fig. 11. First and second derivative of u_{stem} for root-plate damage (2A-D, Fig. 4): $u''d^4$ is the second derivative (Eq. (2)) multiplied by the fourth power of diameter (d_i). u′ is the first derivative (Eq. (3)), h is the stem height. A, B and C are points related to the second derivative deviation due to root-plate damage.

by reporting a 50 or 70 % stiffer model response depending on the soil type. Rahardjo et al. (2014) also explained that there is a 15–25% overestimation of the FE model regarding variability in root and soil properties. The higher *RE* of u_{stem} in the upper part of the stem (above point no. 10, Fig. 6) could be partially caused by an overestimation of stiffness by geometry or material simplification (homogenous material properties over height and tapering derived from the lower part of stem). The *RE's* of $u_{root\text{-}plate}$ calculated for individual markers varied and were relatively high. A higher *RE* was observed for the markers on the edge of the root-plate, which could be explained by the combination of the measured tree root-system irregularities and the influence of the image noise to the small displacements (Sebera et al., 2014). However, the overall character of root-plate deflection (Fig. 6) is comparable between model and measurement. This result is sufficient, considering that the approach was based on representing a heterogeneous real system by using homogenous continuum model. The presented FE model was validated by displacements, strains and inclinations and is considered to be relevant for the sensitivity analysis (*SA*) and the analysis of defects.

4.2. SA outputs

The presented significance of $\boldsymbol{r_2}$ corresponds to the critical role of roots in tree anchorage. Coutts (1986) highlighted the importance of windward root strength. Crook and Ennos (1996) found a positive relationship between anchorage strength and the root cross-sectional area. The significance of root volume was also confirmed by Dupuy et al. (2005) who highlighted root resistance as a function of two of parameters that explained 70 % of the variation by using a combination of biomass and topology. The FE model shows higher influence of r_2 than r_1, which is contrary to the work published by Crook and Ennos (1996), stating that there will be a decrease of strain on the roots the farther they are from the base of the stem. The increasing trend of root volume influence can be given by the lower input range of parameter r_1. In next, the first layer is relatively thin and limited in diameter by the d_b because it is a continuous part of stem. Although the composite root-plate FE model is not based on the real shape and topology of the roots, it still confirms the influence of the role of roots (represented by r_1, r_2) on general anchorage strength. The significance of soil properties described by the FE model is confirmed by Dupuy et al. (2007); Kamimura et al. (2011) and Moore (2000). Also, Coutts (1986) stated that the uprooting process consists of several stages, in which the significance of soil is the most important parameter in the first phase before primary failure. This conclusion agrees with the FE model operating in an elastic range following the elasto-inclino method. The higher impact of $\boldsymbol{E_{soil}}$ in *SA* was involved by defining of relatively wide range of input values.

A higher correlation of $\boldsymbol{hr_2}$ with $u_{root\text{-}plate}$ on the windward side and a lower correlation on the leeward side was observed together with a variation of correlations in regard to distance from stem and should be studied more. However, there can be relation of these differences to the "S" shape of the deformed root-plate surface presented by Villaggio (1998). The significant contribution of the root-plate depth ($\boldsymbol{hr_2}$) and diameter ($\boldsymbol{dr_2}$) is in agreement with the work of Ghani et al. (2009) and Moore (2000). Contrary to Dupuy et al. (2005), who describes the higher significance of root pattern width rather than volume, the results shows higher correlation of $\boldsymbol{E_{soil}}$ and $\boldsymbol{r_2}$. This is also supported by the power effect of thickness on root-plate stiffness according to structural mechanics (Young and Budynas, 2002). The higher significance of $\boldsymbol{E_{soil}}$ and $\boldsymbol{r_2}$ in *SA* corresponds to the wide range of values of input parameters

(Table 1). This can be expected in practice as well, while the correlation between the aboveground and underground geometry parameters is known (Mattheck and Breloer, 2003; Štofko and Kodrík, 2008; Ghani et al., 2009).

In accordance with beam bending theory (Gross et al., 2011) and Sellier and Fourcaud (2009), the $\boldsymbol{d_b}$ has a higher influence on displacements and inclination than $\boldsymbol{E_L}$, even though the $\boldsymbol{d_b}$ varied within a small range (±5%). Therefore, precise *in-situ* measurement that considers the bark thickness (including the upper parts of the stem) is essential for tree response assessment. The stem diameter was found to be significant for the $u_{root\text{-}plate}$ what is caused by the linking of $\boldsymbol{d_b}$ model parameter with root-plate depth (Table 2).

The high correlation of $\boldsymbol{E_L}$ to $\boldsymbol{\varepsilon_{1,2}}$ confirms that extensometers are a valid tool for local measurements of sound wood properties. The local change of E_L influences displacement above the position of change, which affects to overall stem deflection and should be considered during an interpretation of the deflection curve.

4.3. Impact of defects on strains, inclination and deflection curve

The increase in inclination with the size of the root-plate damage corresponds with the experimental findings of Smiley (2008) and Smiley et al. (2014). However, there is some variability among species and even between individual trees that is caused by the size of the roots and their position (Smiley et al., 2014). Representation of root-plate model by composite showed a more direct relationship between the damaged part and increase of θ_1. The influence of defect's position was observed by different inclining θ_2 in the case of 2B and 2C, where the side with damage had a higher inclination. A small decrease in θ_1 due to an increase in stiffness for the stem defect (1A) corresponds to the stem base's 'joint-like' behaviour caused by the defect described by Tippner et al. (2019). However, there is a small increase for the higher located 1B, 1C defects. The response of θ_2 is the opposite for almost all of the stem defects. Based on previously mentioned unclear θ_1, θ_2 reactions, the effect of stem defects on the root-plate inclination and relationship with the position of measurement is not significant. The presented FE results and experiment (Fig. 5a) confirm that inclinometers are a reliable tool as stated by Wessolly and Erb (2016) and Detter et al. (2002). However, the position of the inclinometers while assessing the root-plate damage with asymmetrical location or an irregular stem base is crucial.

Distinctive changes of E_L below the position of evaluation (defect 1A) caused $\varepsilon_{1,2}$ increase. The 1D defect located 1.3 m away from the position of $\varepsilon_{1,2}$ evaluation was shown to have an insignificant impact on $\varepsilon_{1,2}$. When performing a pulling test, it should be taken into consideration that the measurement by extensometers could be influenced by the proximity of defects and the trend in strain distribution could be helpful indicator of defect's position if several extensometers are placed on top of each other. The extensometers capability to sufficiently reveal defects at the same position is confirmed by the increase of $\varepsilon_{1,2}$ (1B, 1C) which corresponds to the research of Ciftci et al. (2014) and Smiley et al. (2012). The higher $\varepsilon_{1,2}$ in the case of 1B indicates that the vertical extension of a defect significantly influences stem stiffness as well as the cross-section extension described by Smiley et al. (2012).

Damage to parts of the root-plate (1B, 1C) caused a decrease of $\varepsilon_{1,2}$ on corresponding sides and an increase on the opposing sides. The stem strains at side with the root-plate damage are lower because of the transfer of internal force by the undamaged, stiffer part of the tree (stem and root-plate connection) which will consequently suffer from higher stress and strains. This confirms the interaction between root-plate and stem stiffness and reveals some path-dependency described by the field study (Tippner et al., 2019) but this should be studied in more detail in the future. Contrary to Brudi and van Wassenaer (2001) and the results of the FE model without defects, the position of the extensometers in the case of a root-plate with one-sided damage could cause inaccurate estimation of stem stability. The placement of extensometers on opposite sides and their interaction between each other and with inclinometers seems to be important. The damage of a fully damaged root-plate (2A) induced only a small increase of $\varepsilon_{1,2}$ on both sides of the stem. The majority of the load probably dissipated for the root-plate's strain and inclination; in principal, the stem strains are not influenced by symmetrical root-plate damage. The connection between the stem and root-plate stiffness should be further investigated more in relation to the evaluation of trees by elasto-inclino method. The supplement of this method by experimental observation of stem deflection could bring sufficient results.

The character of a deflection curve changes with the presence of defects but interpreting this change can be difficult due to the overall curvature of the stem (Fig. 9). The first and second derivative are proposed accordingly to distinguish the effects of a defect. The first derivative changes inclination at the position of the stem defect, but when there is root-plate damage, the whole line shifts. This confirms that the stem inclines more when root-plate damage has occurred, but the shape of the deflection curve is similar to a tree without damage (Fig. 10). The same principle can be observed for stem defects because the inclination of the tree is changed at the location of the defect and the overall displacement increases above where the defect sits. However, bellow and above the defect, the shape of the deflection curve is similar to a tree without defects. This fact is highlighted by second derivative, which shows deviation from the curvature at the position of the stem defect (Fig. 10) and above the root-plate damage (Fig. 11). The high deviation of points revealed by the second derivative also contributed to the visibility of stem deflection, which follows standard behaviour (curvature) above the defect, only with a contribution of displacement caused by defect below. This supports the approach published by Neild and Wood (1999) stating that stem deflection is calculated as the sum of the root-plate inclination and stem displacement. Therefore, the natural course of stem curvature needs to be eliminated by derivations in order to observe the presence of a defect. The combination of the first and second derivative proved to be the best option for the FE study. This approach is suggested for the detection of inner defects by using the optical marker tracking technique.

5. Conclusions

The validated FE model within an elastic range of behaviour provided insight into the principles of tree's mechanical response in regard to root-plate inclination, longitudinal strains in the stem and deflection. During the sensitivity analysis of parameters describing shape and material properties of a tree without defects, the soil properties and root volume were evaluated as the most significant parameters. The analysis of stem defects and root-plate damage confirmed a significant influence of their location according the position of inclination and strain measurement. The extensive damage below the position of strain measurement caused their significant change, while the damage above the position of strain and inclination observation caused only slight change. This interaction between the stem and root-plate stiffness should be considered when the elasto-inclino method is used for tree stability assessment. This means at least two inclinometers and two extensometers should be used for basic measurements and the interaction between these pieces of equipment should be taken into consideration.

Observation of the tree's overall reaction to loading seems to be a crucial point in the understanding of mechanical stability. The multipoint marker tracking technique could be a useful tool but is conditioned by effective data processing. Analysis of the deflection curve showed that the curvature followed the presumed shape according to the beam theory below and above the defect. The deflection curve of the first derivative proved to be an easily accessible evaluation of defect presence. There was a visible change of curve inclination in the case of stem defect and the root-plate damage was presented by the curve offset. This evaluation is supported by the second derivative, in which the defect position was detected by a clear change of curve course. Use of the deflection curve as a potential tool for improving existing methods

should be further confirmed by field studies.

CRediT authorship contribution statement

Barbora Vojáčková: Software, Writing - original draft, Validation, Writing - review & editing. **Jan Tippner:** Supervision, Conceptualization, Methodology, Writing - review & editing, Funding acquisition. **Petr Horáček:** Conceptualization, Supervision. **Václav Sebera:** Investigation, Validation. **Luděk Praus:** Investigation, Writing - review & editing. **Robert Mařík:** Formal analysis. **Martin Brabec:** Investigation.

Declaration of Competing Interest

The authors declare that they have no known competing financial interests or personal relationships that could have appeared to influence the work reported in this paper.

Acknowledgements

The authors gratefully acknowledge the Ministry of Education Youth and Sports in the Czech Republic [Grant Number #LL1909, ERC CZ]; the European Commission for funding the InnoRenew CoE project [Grant Agreement #739574] under the Horizon 2020 Widespread-Teaming program and the Republic of Slovenia (Investment funding of the Republic of Slovenia and the European Union of the European Regional Development Fund). Data for preliminary analyses which contributed to the presented work were measured during Biomechanical Week 2013 founded by International Society of Arboriculture and organized by a number of volunteers.

Appendix 1

Abbreviation	Description	Abbreviation	Description
FE/FEM	Finite element/Finite element method	*Fx*	Force in horizontal direction
DIC	Digital image correlation	*Fz*	Force in vertical direction
RE	Relative error	$M_{(i)}$	Bending moment for corresponding position
SA	Sensitivity analysis	*MOE*	Modulus of elasticity calculated from measured ε_1, ε_2
R^2	Coefficient of determination	E_L, E_R, E_T	Elastic moduli in longitudinal, radial, tangential directions
θ_1	Root-plate inclination at the neutral axis	*EL1*	Longitudinal elastic modulus at stem base
θ_2	Root-plate inclination at the leeward side	*EL2*	Longitudinal elastic modulus to 1 m
ε_1	Strain on the compression side	*EL3*	Longitudinal elastic modulus over 1 m
ε_2	Strain on the tension side	G_{LR},G_{LT}, G_{RT}	Shear moduli
$u_{stem(i)}$	Stem displacement; *(i)* number of observed point	μ_{RL}, μ_{TL}, μ_{TR}	Poisson's ratios
$u_{stem<1m}$	Stem displacement up to 1 m of stem height	E_{soil}	Elastic modulus of soil
$u_{stem1\text{-}1.8m}$	Stem displacement from 1 to 1.8 m of stem height	ρ	Spearman correlation coefficient
$u_{stem>4.5m}$	Stem displacement above 4.5 m of stem height	t	Stem tapering
$u_{root\text{-}plate(i)}$	Displacement on the surface of the root-plate, *(i)* number of observed point	h_{r2}	The depth of static significant root-plate
u_{max}	The maximal displacement at the top of the stem	d_{r2}	The diameter of static significant root-plate
$u''(h_i)$	Second derivative of u_{stem} at the position h_i (Eq. (2))	r_1	Root volume in the first layer
$u'(h_i)$	First derivative of u_{stem} at the position h_i (Eq. (3))	r_2	Root volume in the second layer
$u''d^4$	2nd derivative multiplied by 4th power of diameter at corresponding position	*1A*	Defect at the base of the stem (up to 0.35)
F	Applied load during measurement	*1B*	Defect of the lower part of the stem (up to 2 m)
ht	Height of the cable attachment	*1C*	Defect of the middle part of the stem (from 0.35 to 1 m)
α	Angle of the line anchorage	*1D*	Defect of the upper part of the stem (from 2 to 9.2 m)
d_b	Stem base diameter	*2A*	Damage to the whole root system
d_{bh}	Diameter at breast height	*2B*	Damage on the windward side of the root system
d_e	Diameter at the position of extensometers	*2C*	Damage on the leeward side of the root system
$d_{(i)}$	Diameter of each stem segment at the top part	*2D*	Damage on the 1/4 of the root system on leeward side
$h_{(i)}$	Position along the stem height		
x	Root-plate marker position on the ground		

References

Bowles, J.E., 1997. Foundation Analysis and Design. McGraw-Hill, United States, p. 1207 pp.
Brudi, E., Van Wassenaer, P., 2001. Trees and Statics: Non-Destructive Failure Analysis, pp. 1–17.
Ciftci, C., Kane, B., Brena, S.F., Arwade, S.R., 2014. Loss in moment capacity of tree stems induced by decay. Trees 28, 517–529. https://doi.org/10.1007/s00468-013-0968-8.
Coutts, M.P., 1986. Components of tree stability in sitka spruce on peaty gley soil. Forestry 59, 173–197. https://doi.org/10.1093/forestry/59.2.173.
Crook, M.J., Ennos, A.R., 1996. The anchorage mechanics of deep rooted larch, Larix europea x L-japonica. J. Exp. Bot. 47, 1509–1517. https://doi.org/10.1093/jxb/47.10.1509.
Dahle, G.A., James, K.R., Kane, B., Grabosky, J.C., Detter, A., 2017. A review of factors that affect the static load-bearing capacity of urban trees. Arboric. Urban For. 43.
Detter, V.A., Rust, S., 2013. Aktuelle Untersuchungsergebnisse zu zugversuchen, Findings of recent research on the pulling test method, 2013. Jahrbuch der Baumpflege, pp. 87–100.
Detter, A., Brudi, E., Bischoff, F., Treeconsult, P., Sinn, G., 2002. Statics Integrated Methods, p. 7.
Dupuy, L., Fourcaud, T., Stokes, A., 2005. A numerical investigation into the influence of soil type and root architecture on tree anchorage. Plant Soil 278, 119–134. https://doi.org/10.1007/s11104-005-7577-2.
Dupuy, L.X., Fourcaud, T., Lac, P., Stokes, A., 2007. A generic 3D finite element model of tree anchorage integrating soil mechanics and real root system architecture. Am. J. Bot. 94, 1506–1514.
Ellison, M., 2005. Quantified tress risk assessment used in the management of amenity trees. J. Arboricult. 31, 57–65.
FAO, 2006. Guidelines for Soil Description. Food and Agricultural Organization of the United Nations, p. 97pp.
Fourcaud, T., Ji, J.N., Zhang, Z.Q., Stokes, A., 2008. Understanding the impact of root morphology on overturning mechanisms: a modelling approach. Ann. Bot. 101, 1267–1280. https://doi.org/10.1093/aob/mcm245.
Gaffrey, D., Kniemeyer, O., 2002. The elasto-mechanical behaviour of Douglas fir, its sensitivity to tree-specific properties, wind and snow loads, and implications for stability - a simulation study. J. For. Sci. 48, 49–69.
Ghani, M.A., Stokes, A., Fourcaud, T., 2009. The effect of root architecture and root loss through trenching on the anchorage of tropical urban trees (*Eugenia grandis* Wight). Trees Struct. Funct. 23, 197–209. https://doi.org/10.1007/s00468-008-0269-9.
Gross, D., Hauger, W., Schröder, J., Wall, W.A., Bonet, J., 2011. Engineering Mechanics 2. Mechanics of Materials. Springer-Verlag, Berlin Heidelberg, p. 309 pp.
Jonas, T., Lundström, T., 2005. STEMTRACK Digital Image Analysis As Tool to Detect the Stem Deflection in Tree Stability Experiments: Technical Annex..
Jonsson, M.J., Foetzki, A., Kalberer, M., Lundström, T., Ammann, W., Stöckli, V., 2006. Root-soil rotation stiffness of Norway spruce (*Picea abies* (L.) Karst) growing on subalpine forested slopes. Plant Soil 285, 267–277. https://doi.org/10.1007/s11104-006-9013-7.

Kamimura, K., Kitagawa, K., Saito, S., Mizunaga, H., 2011. Root anchorage of hinoki (*Chamaecyparis obtuse* (Sieb. Et Zucc.) Endl.) under the combined loading of wind and rapidly supplied water on soil : analyses based on tree-pulling experiments. Eur. J. For. Res. 131, 219–227. https://doi.org/10.1007/s10342-011-0508-2.

Khalilnejad, A., Ali, F.H., Hashim, R., 2012. Finite Element Simulation for the Impact of Root Morphology on Pulling-out Process.

Kolařík, J., Janíková, J., Krása, A., Mikita, T., Praus, L., Romanský, M., Šimek, P., Vojáčková, B., Weberová, Š., 2018. Hodnocení stavu stromů SPPK A01 001:2018. Standardy péče o přírodu a krajinu – Arboristické standardy, p. 56 pp..

Kretschmann, D.E., 2010. Wood Handbook. Forest Service.

Lavers, M.G., 1983. The Strength Properties of Timber, 3rd ed. Building Research Establishment, London.

Lundström, T., Jonas, T., Stöckli, V., Ammann, W., 2007. Anchorage of mature conifers: resistive turning moment, root-soil plate geometry and root growth orientation. Tree Physiol. 27, 1217–1227. https://doi.org/10.1093/treephys/27.9.1217.

Mattheck, C., Breloer, H., 2003. The Body Language of Trees, 7th ed. The Stationery Office, Norwich, England, p. 239 pp.

Moore, J.R., 2000. Differences in maximum resistive bending moments of *Pinus radiata* trees grown on a range of soil types. For. Ecol. Manage. 135, 63–71. https://doi.org/10.1016/S0378-1127(00)00298-X.

Mortimer, M.J., Kane, B., 2004. Hazard tree liability in the United States: uncertain risks for owners and professionals. Urban For. Urban Green. 2, 159–165. https://doi.org/10.1078/1618-8667-00032.

Neild, S.A., Wood, C.J., 1999. Estimating stem and root-anchorage flexibility in trees. Tree Physiol. 19, 141–151.

Niklas, K.J., 1992. Plant Biomechanics: An Engineering Approach to Plant Form. The University of Chicago Press, Chicago, p. 607 pp.

Peltola, H.M., 2006. Mechanical stability of trees under static loads. Am. J. Bot. 93, 1501–1511. https://doi.org/10.3732/ajb.93.10.1501.

Rahardjo, H., Harnas, F.R., Indrawan, I.G.B., Leong, E.C., Tan, P.Y., Fong, Y.K., Ow, L.F., 2014. Understanding the stability of *Samanea saman* trees through tree pulling, analytical calculations and numerical models. Urban For. Urban Green. 13, 355–364. https://doi.org/10.1016/j.ufug.2013.12.002.

Riley, K.F., Hobson, M.P., Bence, S.J., 2006. Mathematical Methods for Physics and Engineering, 3rd ed. Cambridge University Press, Cambridge. UK, p. 1333 pp.

Sebera, V., Praus, L., Tippner, J., Kunecky, J., Cepela, J., Wimmer, R., 2014. Using optical full-field measurement based on digital image correlation to measure strain on a tree subjected to mechanical load. Trees 28, 1173–1184. https://doi.org/10.1007/s00468-014-1028-8.

Sebera, V., Kunecký, J., Praus, L., Tippner, J., Horáček, P., 2016. Strain transfer from xylem to bark surface analyzed by digital image correlation. Wood Sci. Technol. 773–787. https://doi.org/10.1007/s00226-016-0819-z.

Sellier, D., Fourcaud, T., 2009. Crown structure and wood properties: influence on tree sway and response to high winds. Am. J. Bot. 96, 885–896. https://doi.org/10.3732/ajb.0800226.

Simon, V., Weighand, B., Gomaa, H., 2017. Dimensional Analysis for Engineers. Mathematical Engineering. Springer Nature, Switzerland, 134 pp.

Smiley, E.T., 2008. Root pruning and stability of young willow oak. Arboric. Urban For. 34 (2), 123–128.

Smiley, E.T., Kane, B., Wesley, R.A., Holmes, L., 2012. Sapwood cuts and their impact on tree stability. Arboric. Urban For. 38 (6), 287–292.

Smiley, E.T., Holmes, L., Fraedrich, B.R., 2014. Arboric. Urban For. 40 (4), 230–236.

Spatz, H.C., Bruechert, F., 2000. Basic biomechanics of self-supporting plants: wind loads and gravitational loads on a Norway spruce tree. For. Ecol. Manage. 135 (1–3), 33–44. https://doi.org/10.1016/S0378-1127(00)00296-6.

Štofko, P., Kodrík, M., 2008. Comparison of the root system architecture between windthrown and undamaged spruces growing in poorly drained sites. J. For. Sci. 54, 150–160.

Sutton, M.A., Orteu, J.J., Schreier, H.W., 2009. Digital Image Correlation for Shape and Deformation Measurement Basic Concepts, Theory and Applications. Springer-Verlag, Heidelberg, p. 322 pp.

Szoradova, A., Praus, L., Kolarik, J., 2013. Evaluation of the root system resistance against failure of urban trees using principal component analysis. Biosyst. Eng. 115, 244–249. https://doi.org/10.1016/j.biosystemseng.2013.03.001.

Tippner, J., Praus, L., Brabec, M., Sebera, V., Vojáčková, B., Milch, J., 2019. Using 3D digital image correlation in an identification of defects of trees subjected to bending. Urban For. Urban Green. 46, 1–10. https://doi.org/10.1016/j.ufug.2019.126513.

Villaggio, P., 1998. The roots of trees. Contin. Mech. Thermodyn. 10, 233–240. https://doi.org/10.1007/s001610050090.

Vojáčková, B., Tippner, J., Horáček, P., Praus, L., Sebera, V., Brabec, M., 2019. Numerical analysis of branch mechanical response to loading. Arboric. Urban For. 45, 120–131.

Wessolly, L., 1995. Fracture diagnosis of trees, part 1: statics-integrated methods - measurement with tension test. Stadt und Grün 6, 416–422.

Wessolly, L., 1996. Stability of trees, explanation of the tipping process. Stadt und Grün 4, 268–272.

Wessolly, L., Erb, M., 2016. Tree Statics and Tree Inspection. Patzer Verlag, Berlin – Hanover, p. 288 pp.

Yang, M., Défossez, P., Danjon, F., Fourcaud, T., 2014. Tree stability under wind: simulating uprooting with root breakage using a finite element method. Ann. Bot. 114, 695–709. https://doi.org/10.1093/aob/mcu122.

Young, W.C., Budynas, R.G., 2002. Roarks's Formulas for Stress and Strain, 7th ed. McGraw-Hill Professional, p. 852 pp.